JACS Au
AN OPEN ACCESS JOURNAL OF THE AMERICAN CHEMICAL SOCIETY

pubs.acs.org/jacsau

Article

Cooperative Activation of Cellulose with Natural Calcium

Gregory G. Facas,[‡] Vineet Maliekkal,[‡] Cheng Zhu, Matthew Neurock, and Paul J. Dauenhauer*

Cite This: *JACS Au* 2021, 1, 272–281

Read Online

ACCESS | Metrics & More | Article Recommendations | Supporting Information

ABSTRACT: Naturally occurring metals, such as calcium, catalytically activate the intermonomer β-glycosidic bonds in long chains of cellulose, initiating reactions with volatile oxygenates for renewable applications. In this work, the millisecond kinetics of calcium-catalyzed reactions were measured via the method of the pulse-heated analysis of solid and surface reactions (PHASR) at high temperatures (370–430 °C) to reveal accelerated glycosidic ether scission with a second-order rate dependence on the Ca^{2+} ions. First-principles density functional theory (DFT) calculations were used to identify stable binding configurations for two Ca^{2+} ions that demonstrated accelerated transglycosylation kinetics, with an apparent activation barrier of 50 kcal mol^{-1} for a cooperative calcium-catalyzed cycle. The agreement of the mechanism with calcium cooperativity to the experimental barrier (48.7 ± 2.8 kcal mol^{-1}) suggests that calcium enhances the reactivity through a primary role of stabilizing charged transition states and a secondary role of disrupting native H-bonding.

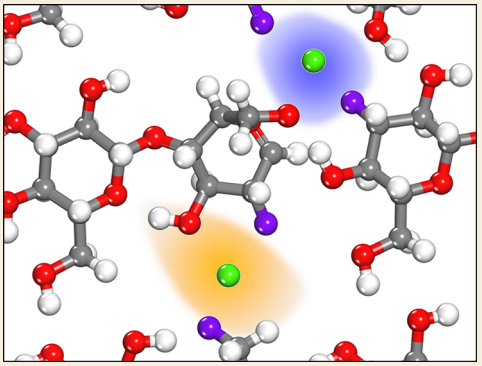

KEYWORDS: *Activation, Cellulose, Calcium, Hydrogen Bond, Glycosidic Bond, Cyclodextrin*

INTRODUCTION

The thermochemical conversion of biopolymers such as cellulose renewably produces an array of five- or six-carbon oxygenates that can be catalytically upgraded to fuels and chemicals.[1−3] The maximum yield of oxygenates, including levoglucosan, furans, and pyrans, is produced at temperatures between 400 and 600 °C where cellulose activates to form volatile components sufficiently quickly to evaporate organic compounds from the reacting molten cellulose.[4−7] While progress has been made to develop models of cellulose reaction kinetics, most notably by Broadbelt and co-workers,[8,9] experimental kinetics to support cellulose fragmentation mechanisms have been difficult to obtain due to the challenges in quantifying hundreds of compounds forming over milliseconds from the complex, evolving the macromolecular structure of the reacting cellulose.[10−12] These experimental challenges have limited the development of a detailed understanding of the activation mechanisms of cellulose and the more complicated catalytic role of naturally occurring alkaline-earth and alkali metals in lignocellulosic materials.[10]

High-temperature cellulose activation occurs via the intermonomer scission of chains that are interconnected by a network of hydrogen bonds (H-bonds), as depicted in Figure 1A. Transglycosylation is widely believed to be the dominant one-chain scission mechanism, which involves the nucleophilic attack of the C6 hydroxymethyl group of the cellulose monomer on the C1 carbon, thereby breaking the glycosidic ether bond and the cellulose chain with a calculated activation barrier of 50–53 kcal mol^{-1} in the absence of intrasheet H-bonding.[9,13,14] By this mechanism, the C6 hydroxymethyl group must be free to rotate close to the C1 carbon; in the crystalline structure of cellulose Iβ, Hosoya et al. calculated that breaking the H-bonds connected to the C6 hydroxymethyl group can increase the transglycosylation activation barriers by almost 10 kcal mol^{-1}.[15] Westmoreland and co-workers, on the other hand, computed a lower activation energy for transglycosylation catalyzed by water and small oxygenates that are H-bonded to the reacting carbohydrates, lowering the activation energy to around 36–40 kcal mol^{-1}.[16] Auerbach and co-workers similarly showed that precursors to levoglucosan can be formed with free-energy barriers of ∼36 kcal mol^{-1} via transition states that are stabilized by H-bonding.[17]

Recent experimental kinetics to further characterize cellulose activation revealed the role of the H-bonding network in cellulose chemistry.[18,19] Experimental measurements indicated two kinetic regimes that transition at 467 °C.[18] At high temperatures, cellulose activates with an apparent energy of 53.7 ± 1.1 kcal mol^{-1} (prefactor of 2.4×10^{16} s^{-1}), which is consistent with the uncatalyzed transglycosylation mechanism. However, below 467 °C the apparent activation energy for cellulose activation was measured to be significantly lower at 23.2 ± 1.9 kcal mol^{-1} (prefactor of 2.0×10^{7} s^{-1}), indicating that the reaction is driven via a seemingly catalytic mechanism

Received: November 27, 2020
Published: February 22, 2021

https://dx.doi.org/10.1021/jacsau.0c00092
JACS Au 2021, 1, 272–281

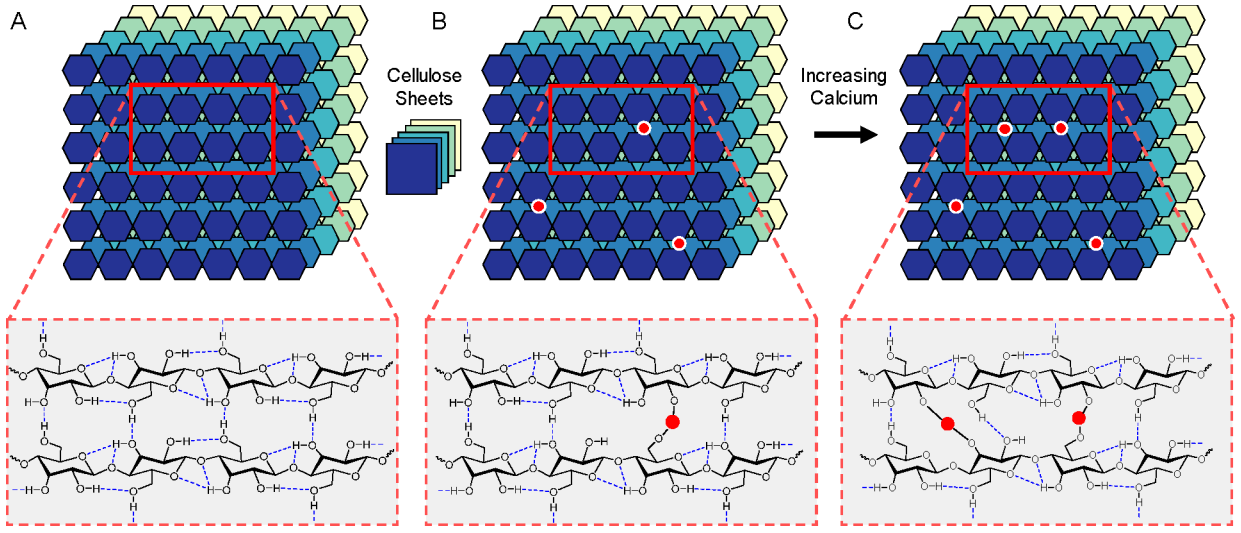

Figure 1. (A) Cellulose consists of long chains of $\beta(1-4)$ linked D-glucose units that are hydrogen-bonded to form stackable sheets. (B) Introduction of calcium ions (depicted here as red spheres) into the cellulose matrix disrupts the native hydrogen-bonding network, leading to increased the reactivity of the cellulose chains. (C) Higher loadings of calcium produce neighboring calcium binding sites capable of cooperatively catalyzing the scission of intermonomer glycosidic bonds.

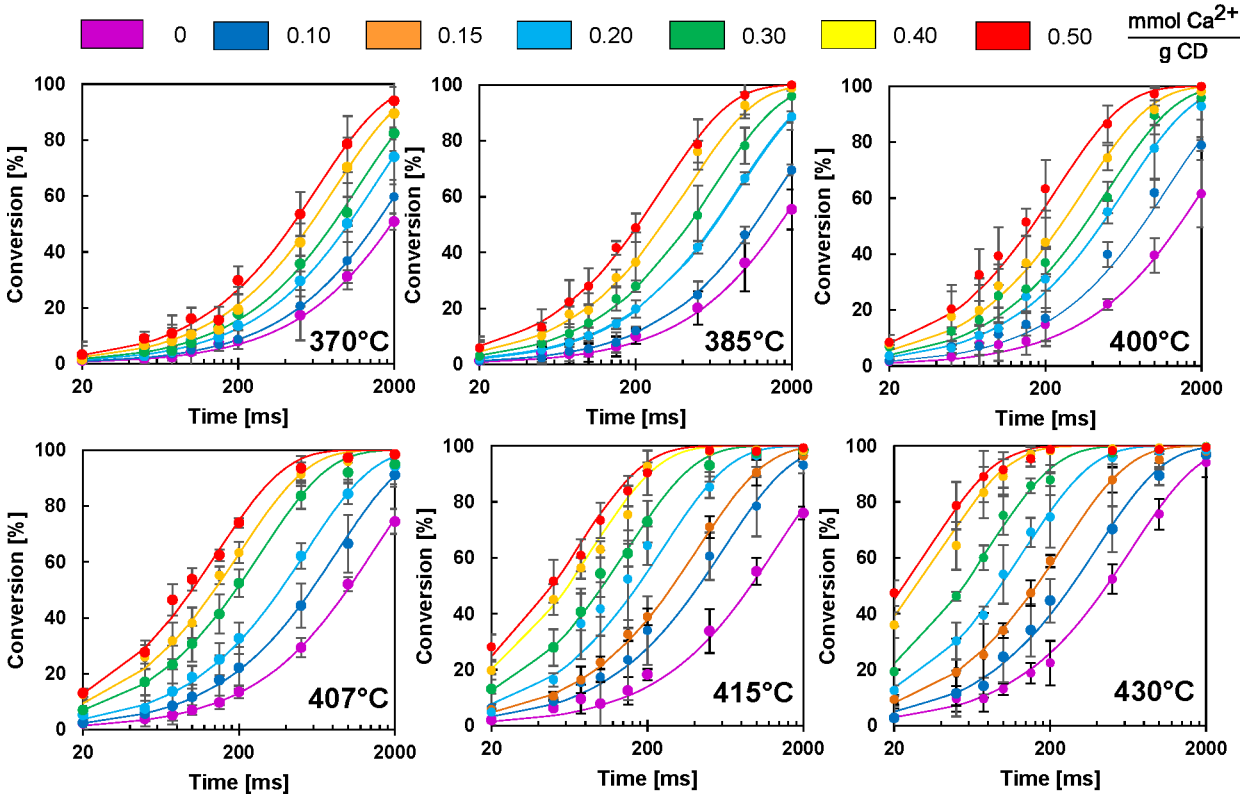

Figure 2. Kinetics of the cellulose surrogate, α-cyclodextrin, with a calcium catalyst. The thermal activation of cyclodextrin was measured by determining conversion of cyclodextrin with various loadings of the Ca^{2+} catalyst (0–0.50 mmol Ca^{2+} g_{CD}^{-1}) and at various temperatures (370–430 °C) using the pulse-heated analysis of solid and surface reactions (PHASR). All experimental conditions exhibited first-order kinetics in cyclodextrin, and the conversion (●) fit to a first-order model (−). Error bars represent 95% confidence intervals based on triplicate runs.

that occurs within the cellulose molten phase even in the absence of any added catalyst. This lower apparent barrier was consistent with computed energies for a mechanism where vicinal hydroxyl groups on neighboring cellulose chains promote facile proton transfer during transglycosylation, thus leading to a hydroxyl-catalyzed mechanism.[19] These studies indicate that H-bonding in the vicinity of the reaction center can increase or decrease the activation kinetics depending on the conditions, i.e., solid crystal versus reacting melt, respectively, as has been noted in a recent review by Westmoreland.[20] Such a significant influence of the H-bonding environments has been observed and is also prevalent in other biomass conversion reactions, particularly in the acid-catalyzed conversion of biomass-derived sugars.[21,22]

https://dx.doi.org/10.1021/jacsau.0c00092
JACS Au 2021, 1, 272–281

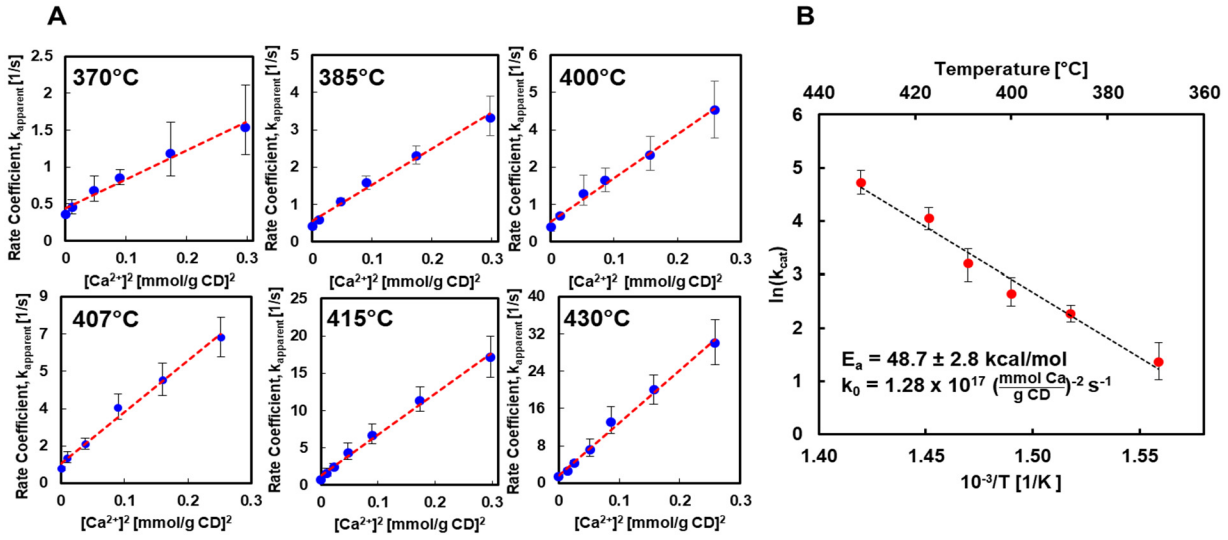

Figure 3. (A) Comparison of apparent first-order rate parameters of the calcium-catalyzed cyclodextrin glycosidic bond activation to the square of the calcium concentration. The linear fit at all temperatures indicates the second-order dependence of the calcium concentration on the rate of activation. (B) Catalyzed activation rate constants in the Arrhenius form; error bars represent 95% confidence intervals.

Alternatively, the vicinal hydroxyl reaction environment in cellulose can also be modified by the presence of natural metal impurities. Lignocellulosic feedstocks have varying amounts of alkaline-earth (Mg^{2+} and Ca^{2+}) and alkali (Na^{+} and K^{+}) metals, which chemically influence both the composition of the final product yields and the overall rate of cellulose breakdown.[23−28] Cellulose breakdown studies using thermal analysis techniques such as TGA and DSC showed that these metals reduce the onset temperature where cellulose degradation occurs.[25] In a homogeneous catalysis for biomass upgrading, metal ions are known to significantly reorient solvent H-bonds in their vicinity.[29] Similarly, metal cations with +1 or +2 oxidation states are expected to selectively bind to different regions of the cellulose matrix and disrupt the H-bonding environment in a manner similar to that of homogeneous catalysis carried out in metal salt solutions. In addition, the Lewis acid character of these metals can stabilize the oxygenated transition states.[30−32] While the many studies reported above have quantified metal-catalyzed products, the experiments only measured product yields at full conversion (no kinetics) and convoluted primary and secondary reactions.

In this work, the mechanism of calcium-promoted cellulose activation is evaluated by combined experimental reaction kinetic studies and first-principles density functional theory (DFT) calculations to identify favorable metal binding positions and elucidate the catalytic activation mechanism. The activation kinetics of calcium catalysis were measured by the pulse-heated analysis of solid and surface reactions (PHASR) by rapidly heating and cooling a film of cellulose at a temporal resolution as small as 20 ms.[33] As shown by previous experiments, PHASR provides temporally resolved reaction kinetic data in the absence of heat and diffusion transport artifacts, thereby facilitating reliable comparisons between experimental kinetic data and ab initio calculated activation barriers.[11,33,34] The activation mechanism was characterized by the reaction of calcium-impregnated α-cyclodextrin (CD). CD is a known kinetic surrogate of cellulose that is readily quantified[35] (also refer to Supplemental Note 1) and exhibits similar computed barriers for activation as those of cellulose despite having a different C1 stereochemistry.[36] Experimental kinetics were measured at varying temperatures (370−430 °C) and calcium concentrations (0.1−0.5 mmol Ca^{2+} g_{CD}^{-1}). The experimental results were used along with DFT studies to elucidate the primary catalytic role of calcium in aiding C−O bond scission as well as a secondary role where calcium contributes to disrupting H-bonding networks (Figure 1B and C). This work presents the first such study on intrinsic cellulose activation kinetics in the presence of metal salts and highlights the unique roles that metal ions can play in enhancing reactivity.

RESULTS AND DISCUSSION

Experimental Reaction Kinetics

The temporal extent of conversion of α-cyclodextrin was measured for thermal pulses of 20−2000 ms, temperatures of 370−430 °C, and calcium concentrations of 0.1−0.5 mmol Ca^{2+} g_{CD}^{-1} as depicted in Figure 2. Each data point is comprised of at least three independent experimental trials, and the error bars associated with each point represent a 95% confidence interval. The conversion of α-cyclodextrin exhibited an apparent first-order kinetic behavior with respect to the α-cyclodextrin mass among all temperatures and calcium concentrations. For each temperature and concentration series, a first-order kinetic model was fit to the experimental data and was found to pass through all the experimental confidence intervals. At 415 °C, pure α-cyclodextrin only achieved a ∼75% conversion after a reaction duration of 2000 ms. In contrast, when α-cyclodextrin was doped with 0.5 mmol Ca^{2+} g_{CD}^{-1} at 415 °C, a similar conversion was achieved within 100 ms and an exceeded a conversion of 90% was achieved within 200 ms (see Tables S1A−M)

The experimental data presented in Figure 2 show that calcium significantly increased the overall decomposition kinetics of cyclodextrin. To ensure that Ca^{2+} was the catalytic material, experiments were also conducted with different calcium salts, $Ca(NO_3)_2$ and $CaCl_2$ (Figure S3-1); these experiments indicated that the overall measured kinetics were independent of the identity of the counterion (NO_3^- or Cl^-). This was further evaluated by thermogravimetric analysis with

https://dx.doi.org/10.1021/jacsau.0c00092
JACS Au 2021, 1, 272−281

mass spectrometry, where these anions were shown to volatilize out of the cellulose matrix at temperatures lower than the reaction temperature (Figure S3-2). This agrees with other recent studies that suggest anions are not present in the reaction melt at reaction conditions.[37] Based on these findings, we propose that Ca^{2+} is responsible for catalysis, and the counterions are not present near the reaction center.

To characterize the effect of the calcium catalyst, the experimental conversion data of Figure 2 were fit to a first-order kinetic model with apparent rate parameters, k_{app} (see eq 1), for each temperature and calcium concentration. The first-order rate parameters were then plotted against the varying integer powers of the calcium concentration to determine the dependence of the calcium concentration on the rate of activation. The apparent rate parameters exhibited an almost linear fit with respect to the square of the calcium concentration as shown in Figure 3A, indicating a second-order rate dependence on the catalyst concentration. In addition, a noninteger fit was conducted to evaluate the rate order, as shown in Figure S5−1. The slope of the fit line in these plots suggests a rate order of 1.71 ± 0.09, thus indicating a near-second-order rate dependence. It must be noted that while a non-first-order dependence on the catalyst concentration is typically not measured in heterogeneous catalysis, such rate orders are found in homogeneous systems. For example, Bures discussed case studies where the participation of reactant-metal complexes in bimolecular reactions resulted in a second-order rate dependence on the catalyst concentration.[38] Other studies have also observed first- and second-order dependencies on the catalyst concentration.[39] As shown, the rate coefficient was nonzero at a zero calcium concentration, which is consistent with uncatalyzed cellulose chemistry as previously measured.[18] For comparison, other rate expressions were evaluated, as shown in Figure S4-1 of the Supporting Information.

From a mechanistic standpoint, the second-order rate dependence in calcium concentration suggests a catalytic mechanism that proceeds via two calcium ions in the elementary steps. The rate of activation can then be described as

$$\text{rate of reaction } (g_{CD}\, s^{-1}) = k_{app} \times M_{CD} = (k_H + k_C[Ca^{2+}]^2) \times M_{CD} \quad (1)$$

where k_H is a homogeneous or noncatalyzed rate constant, kC is a catalyzed rate constant, and M_{CD} is the mass of α-cyclodextrin. Mass was chosen instead of concentration because α-CD is a kinetic surrogate for cellulose and it is difficult to characterize the concentration of cellulose. This model was selected to incorporate the first-order kinetic behavior with respect to the α-cyclodextrin mass at all calcium concentrations (Figure 2), the second-order dependence on calcium, and the nonzero rate of reaction when calcium is not present with the homogeneous rate-constant term. The catalyzed rate constant, k_C, was determined by fitting to the model described above and is presented in Arrhenius form in Figure 3B. The second-order kinetic catalytic rate constant exhibits a high activation energy, E_a = 48.7 ± 2.8 kcal mol^{-1}, and a pre-exponential factor k_0 = 1.28 × 10^{17} (mmol Ca $g_{CD}^{-1})^{-2}$ s^{-1} (1.35 × 10^{17} (mole Ca per mole CD)$^{-2}$ s^{-1} on a mole per mole basis). It must also be noted that the use of activities is more appropriate in the presence of salts than the use of concentrations. While models exist for the prediction of the activity coefficients of salts in electrolyte or aqueous solutions,[29] predictive models are not currently available for polymer solids or melts. Therefore, we will continue to use concentrations throughout the analysis of the manuscript.

Previous work utilizing PHASR considered the activation of pure cellulose by measuring the conversion of α-cyclodextrin between 385 and 505 °C, which indicated a significant change in the rate of activation above 467 °C.[18] As discussed in the introduction, this two-kinetic regime behavior was attributed to a noncatalyzed transglycosylation mechanism at high temperatures and a hydroxyl-catalyzed transglycosylation mechanism at low temperatures.[19] This two-regime behavior motivated the plotting of the total reaction rate constant (k_{app} in eq 1) for the conversion of α-cyclodextrin at different calcium concentrations on an Arrhenius plot, as shown in Figure 4. The dashed colored lines in Figure 4 represent fit lines for the rate constants that combine contributions from the homogeneous rate constant (in the absence of calcium) and the calcium-catalyzed rate constant using the measured activation energies and associated Arrhenius pre-exponential factors. Figure 4 reveals the absence of any sharp transition at the chosen temperatures and calcium concentrations, which is likely due to the inclusion of contributions from the calcium-catalyzed rate constant that was shown to display just one regime at all temperatures (Figure 3B). Furthermore, it was observed that the slope of the line tends toward the slope of the calcium-catalyzed pathway at higher calcium concentrations. This suggests that the contribution of the calcium-catalyzed mechanism becomes dominant at higher catalyst concentrations.

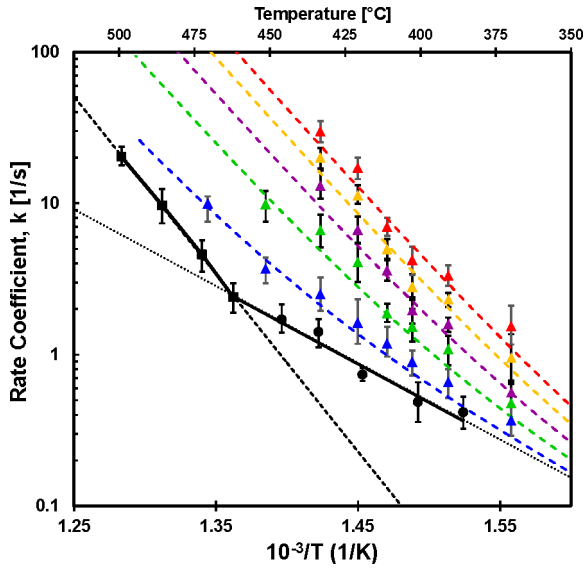

Figure 4. Global interpretation of calcium-catalyzed cellulose activation. Arrhenius plot of uncatalyzed (black) and catalyzed (colored) cellulose activation for calcium loadings of 0.1 (blue), 0.2 (green), 0.3 (purple), 0.4 (orange), and 0.5 (red) mmol Ca^{2+} g_{CD}^{-1}. Dashed colored lines represent a fit for the activation rate constant with contributions from both the catalyzed and uncatalyzed activation. Error bars represent 95% confidence intervals.

An explanation for the observed kinetics and the approximately second-order dependence of the calcium concentration is provided via a theoretical analysis of the

https://dx.doi.org/10.1021/jacsau.0c00092
JACS Au 2021, 1, 272−281

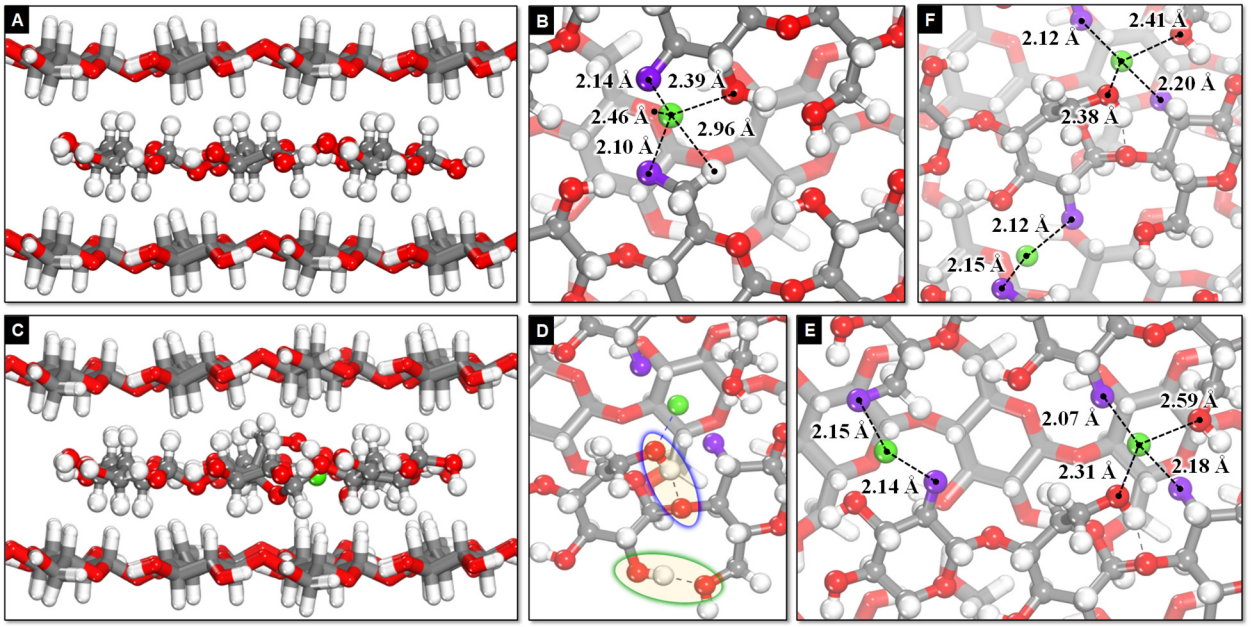

Figure 5. (A) Computational model for a neat reactant consisting of two extended sheets (shown in stick form) and a reacting sheet (in ball and stick form). (B) Optimized structure of the most-stable binding site for calcium. The active site consists of the metal ion, a Lewis acid site, and two deprotonated hydroxyl groups, which are Lewis base sites (purple). (C) Front view of the bound reactant with a single calcium ion. (D) Zoomed-in top view of the bound reactant with a single primary calcium ion. The hydroxymethyl group must rotate out of plane to form a hydrogen bond with the glycosidic oxygen atom for the reaction to occur (circled blue). Breaking intramolecular hydrogen bonds (circled green) can promote facile intermonomer scission. (E) In configuration 1, a second calcium ion facilitates the rotation of the hydroxymethyl group. (F) In configuration 2, a second calcium ion disrupts an intramolecular hydrogen bond.

calcium-catalyzed activation mechanisms using cellulose. In previous studies, it was shown that the C1 stereochemistry of glycosidic bonds (C1−O−C6) does not influence the kinetics of activation[36] or the distribution of decomposition products;[35] cyclodextrin (α-glycosidic bonds) and cellulose (β-glycosidic bonds) both produced the same chemical products at the same rate. Comparable behavior resulted from similar mechanisms of nucleophilic attack in hydroxyl groups that activated glycosidic bonds.[36] As such, computed mechanisms evaluating the calcium-catalyzed activation considered the β-glycosidic bonds of cellulose.

Nature of Calcium Active Sites

Prior studies have suggested that metal ions can form chelated complexes with the hydroxyl groups of cellulose chains, which could be active sites for catalysis.[30−32] While these proposed sites or complexes may be stable binding sites for metal ions at ambient conditions, the experiments reported here (Supplemental Note S3 and Figure S3-1 and 2) suggest that the anions leave the polymer melt as volatile acids at the reaction conditions. This indicates that the source providing protons to leave with the anions is likely the hydroxyl groups of the cellulose chains. In the absence of these protons, the deprotonated hydroxyl groups would likely be stabilized by calcium ions, leading to a Lewis acid (LA)−Lewis base (LB) site pair comprised of the calcium cation (LA) and the oxygen anion (LB) of the deprotonated hydroxyl.

A suitable model that represents the cellulose Iβ crystal (Figure 5A) was used to identify stable binding positions for the metal cations. A single calcium ion in this system corresponds to ∼1.0 wt %, which is within the experimental range for the calcium concentration. Various different binding sites were examined within the cellulose matrix, as outlined in the Supporting Information. The most stable binding site (based on electronic energies) for calcium, as well as the resting state of the catalyst, is a site that sits between the deprotonated states of C6 and C3 hydroxyl groups of two adjacent chains, thus forming a stable O−Ca−O bridge; this binding site is more stable than any other binding site by 2−8 kcal mol^{-1} (structures of other sites are shown in Figure S6-1) The bond lengths for the Ca−O bonds shown in Figure 5B are in good agreement with XRD studies of calcium-impregnated sugar crystals.[40,41]

To evaluate the mobility of calcium ions and address the mechanism for calcium ion diffusion, a mechanism was first developed wherein a hydroxyl group from a vicinal sugar transfers its proton to a deprotonated bridging O anion and binds to the calcium ion. Through this mechanism, calcium ions can move from site to site via small molecules that contain hydroxyl groups. We verified this using a simple model of glucose molecules interacting with an O−Ca−O bridged site and calculated a very low barrier of 2.5 kcal mol^{-1}, which suggests facile diffusion. It is expected that such hydroxyl group interactions with calcium binding sites would be easier in a melt phase, as small molecules in the melt can interact and move around more freely. Therefore, a periodic model was used that consisted of two cellulose sheets containing the impregnated calcium, with glucose and water molecules being used to fill the space in between to signify trapped melting regions. This is a simple model to begin to explore cation transport via trapped lighter products and hydroxyl groups of sugars within the melt. Ab initio molecular dynamics simulations on these prototypical models showed that the calcium ions can indeed easily move from bridged sites into the melt phase in short time scales of 15 ps (further details on the diffusion are available in Supplemental Note S7)

https://dx.doi.org/10.1021/jacsau.0c00092
JACS Au 2021, 1, 272−281

Scheme 1. Mechanism for Glycosidic Bond Cleavage by Transglycosylation Catalyzed by a Single Calcium Ion[a]

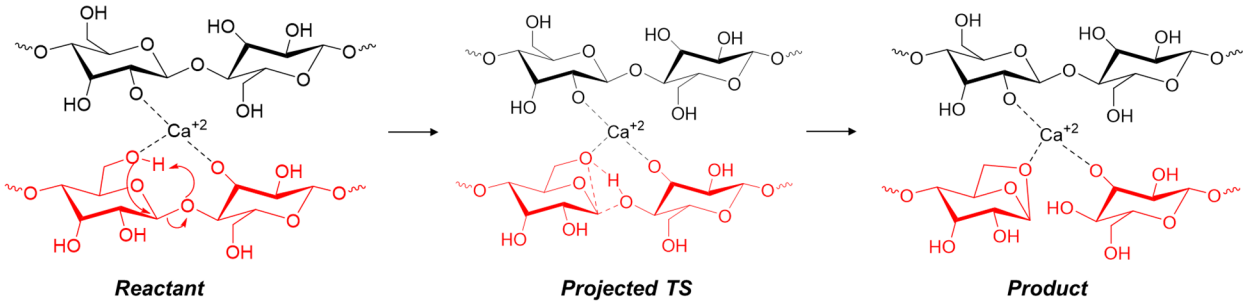

[a]Monomers shown in red correspond to monomers connected by a glycosidic bond that undergoes catalytic cleavage.

A rate-order dependence on the calcium concentration that is nearly second-order suggests that a mechanism with two calcium ions is likely the dominant mechanism under these reaction conditions. However, this may not be true at all calcium concentrations; for the sake of completeness, we consider the following two mechanisms: a single calcium ion mechanism and a dual-calcium ion mechanism for cellulose activation. The first mechanism involves the participation of a single calcium ion

$$\mathrm{Ca} + \mathrm{Cell} \overset{K_1}{\leftrightarrow} \mathrm{Ca{-}Cell} \tag{2}$$

$$\mathrm{Ca{-}Cell} \overset{k}{\rightarrow} \mathrm{Ca{-}Int} \tag{3}$$

$$\mathrm{Ca{-}Int} \overset{K_2}{\leftrightarrow} \mathrm{Ca} + \mathrm{Int} \tag{4}$$

where Cell is the neat cellulose chain, Int is the post-cleavage intermediate, Ca is the calcium catalyst, and Ca−Cell is the calcium-bound intermediate. The constants k, K_1, and K_2 refer to the intrinsic rate constants for glycosidic bond cleavage of the cellulose, adsorption of the cellulose to the Ca, and desorption of the intermediate from the Ca, respectively. The rate that is thought to be controlled by glycosidic cleavage can be written as

$$\text{rate} = \frac{kK_1 \times [\mathrm{Cell}][\mathrm{Ca}_{\mathrm{initial}}]}{(1 + K_1[\mathrm{Cell}])} \tag{5}$$

where the rate dependence of calcium will be first order if the first term in the denominator is dominant (i.e., the unbound cellulose state is abundant). Considering that the most stable binding site for calcium is not near the reaction center (Figure 5B), it is reasonable to assume that the unbound cellulose reaction center is the abundant species. Panels C and D of Figure 5 show the front and zoomed-in top view, respectively, of the bound Ca−Cell intermediate where the calcium ion closely interacts with the hydroxymethyl group and the glycosidic oxygen. In such a configuration, calcium can stabilize the transition state and catalyze the transglycosylation reaction (Scheme 1) believed to be a dominant initiation mechanism, thus leading to a levoglucosan chain-end intermediate (i.e., the product in Scheme 1 (Int)).[9,13,14]

Looking more closely at Figure 5D, the rotation of the C6 hydroxymethyl group needed to interact with the glycosidic bond (circled blue), which is critical for transglycosylation, requires breaking multiple intrasheet H-bonds, leading to an energy penalty. This penalty has been shown to increase the activation barriers of transglycosylation from 51 to 53 kcal mol^{-1} in simple gas-phase models to ∼59 kcal mol^{-1} for such crystal models.[15] Similarly, there exists a strong intramolecular H-bond that needs to be stretched or broken during the course of the reaction (circled green in Figure 5D). It is therefore possible for an additional calcium ion to bind in configurations such as those shown in Figure 5E and F and disrupt native H-bonding networks, leading to potentially lower barriers. The two configurations for cooperative calcium catalysis shown in Figure 5E and F are referred to as configurations 1 and 2, respectively. In these scenarios, an alternative catalytic cycle can be proposed as follows:

$$\mathrm{Ca} + \mathrm{Cell} \overset{K_1}{\leftrightarrow} \mathrm{Ca} - \mathrm{Cell} \tag{6}$$

$$\mathrm{Ca} + \mathrm{Ca{-}Cell} \overset{K_2}{\leftrightarrow} \mathrm{Ca{-}Cell{-}Ca} \tag{7}$$

$$\mathrm{Ca{-}Cell{-}}Ca \overset{k}{\rightarrow} \mathrm{Ca{-}Int{-}Ca} \tag{8}$$

$$\mathrm{Ca{-}Int{-}Ca} \overset{K_3}{\leftrightarrow} \mathrm{Ca} + \mathrm{Ca{-}Int} \tag{9}$$

$$\mathrm{Ca{-}Int} \overset{K_4}{\leftrightarrow} \mathrm{Ca} + \mathrm{Int} \tag{10}$$

where Ca−(X) and Ca−(X)−Ca are the single- and double-bound calcium intermediates, respectively. This model yields a rate expression for the slowest step as follows:

$$\text{rate} = \frac{kK_1K_2 \times [\mathrm{Cell}][\mathrm{Ca}_{\mathrm{initial}}]^2}{(1 + K_1[\mathrm{Cell}])^2} \tag{11}$$

The proposed catalytic cycle would lead to the second-order rate dependence of calcium ion the rate of activation when the concentrations of Ca-bound species are low. Detailed derivations of the above rate expressions as well as the concentration balances on Ca are provided in Supplemental Note S8.

The two calcium-catalyzed mechanisms can be combined with the noncatalyzed activation mechanism to form a single model (see Supplemental Note S8). An overall rate expression for such a unified model would give

$$\text{rate} = k_{\mathrm{H}}[\mathrm{Cell}] + k_1[\mathrm{Ca{-}Cell}] + k_2[\mathrm{Ca{-}Cell{-}Ca}] \tag{12}$$

where k_{H} is the rate constant for the noncatalyzed reaction step, k_1 is the rate constant for the single-calcium-catalyzed reaction step, and k_2 is the rate constant for the cooperative calcium-catalyzed reaction step. Using a similar derivation and similar assumptions about the concentration of the calcium bound species, a simplified rate expression could be derived as follows:

$$\text{rate} = k_{\mathrm{H}}[\mathrm{Cell}] + k_{\mathrm{app1}} \times [\mathrm{Cell}][\mathrm{Ca}_{\mathrm{initial}}] + k_{\mathrm{app2}} \times [\mathrm{Cell}][\mathrm{Ca}_{\mathrm{initial}}]^2 \tag{13}$$

https://dx.doi.org/10.1021/jacsau.0c00092
JACS Au 2021, 1, 272−281

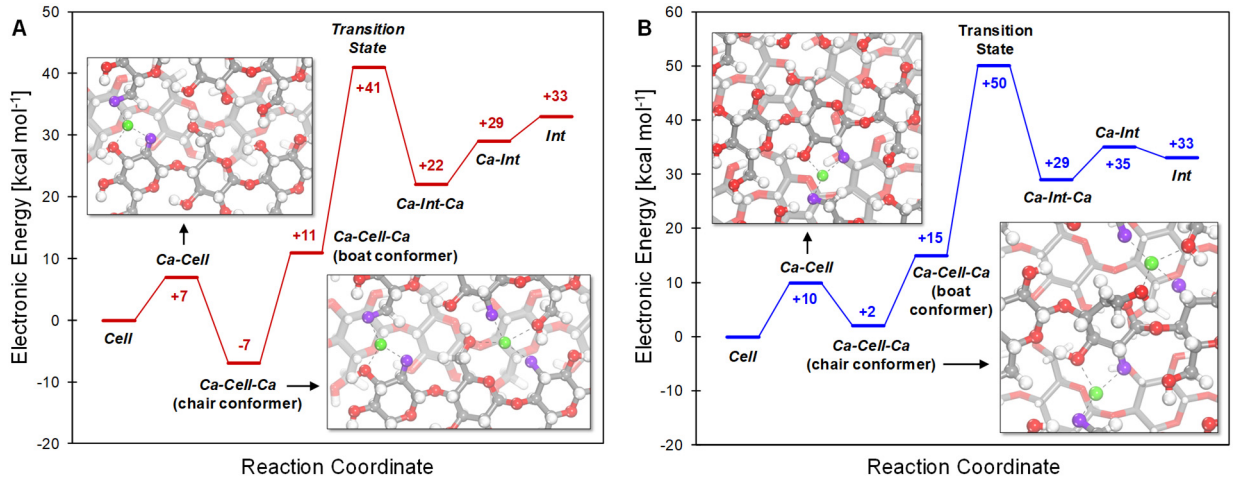

Figure 6. Reaction energy profile for the dual-calcium-catalyzed transglycosylation reaction of cellulose. (A) Configuration 1 with two calcium ions. (B) Configuration 2 with two calcium ions. It must be noted that in both cycles the reference state (0 kcal mol^{-1}) is the Cell + 2Ca state. The absolute energy of this state is equal to the energy of the neat cellulose reactant model plus two times the energy of the calcium bound in its most stable site (shown in Figure 5B). In subsequent bound intermediates, the calcium ions are brought in from the most stable binding states to bind to the reaction center.

Since α-cyclodextrin is a kinetic surrogate for cellulose, one can equivalently modify eq 13 to obtain a rate expression for cyclodextrin as well

$$\text{rate of CD consumption} = (k_H + k_{app1} \times [Ca_{initial}] + k_{app2} \times [Ca_{initial}]^2) * M_{CD} \quad (14)$$

Such an overall expression could lead to a rate-order dependence of ~1.7 depending on the relative magnitude of the three kinetic terms. The proposed roles of the calcium associated with the rate constants, k_{app1} and k_{app2}, were evaluated via DFT first for the single-calcium activation mechanism and then for configurations 1 and 2 of the dual-calcium activation mechanism.

DFT-Calculated Energetics for Calcium Catalytic Cycles

All optimized structures and transition states discussed in this section were isolated using static DFT calculations. The "Ca" state refers to calcium bound to the most stable state (discussed earlier). Subsequent Ca-bound reactive species are formed by moving calcium from this most stable state to the reaction center.

First, considering the energetics of the single calcium catalytic cycle in Figure S9-1, it is shown that the binding of Ca to form the Ca−Cell reactant in the boat conformer (necessary to carry out transglycosylation) is 17 kcal mol^{-1} uphill in energy. This uphill energetic penalty is derived from two sources: (1) the penalty required to move the calcium ion from its most favorable binding site to the site where it carries out catalysis and (2) the energetic penalty required to break intrasheet H-bonds to rotate the hydroxymethyl group to drive the transglycosylation. At low concentrations of Ca bound to the active site, the apparent rate constant for transglycosylation from cycle 1 is $k_{app} = kK_1$. This results in a calculated apparent activation energy of 53 kcal mol^{-1}, which is lower than the barrier for carrying out transglycosylation in a neat cellulose crystal (59 kcal mol^{-1}).[19] This leads to the observation that one of the primary roles of calcium in this chemistry is to stabilize the negatively charged hydroxymethyl O6 atom in the transition state. This cycle would result in a rate-order dependence of one and an activation barrier of 53 kcal mol^{-1}.

Having studied the single-calcium catalytic mechanism, we now move to the dual-calcium mechanism. Considering the energetic cycle for activation configuration 1 with two calcium ions (Figure 6A), the energy diagram indicates an energetic penalty (+7 kcal mol^{-1}) to move a calcium ion from its most favorable binding site (Figure 5B) to the site in Figure 5E where it disrupts the native H-bonding and facilitates the movement of the hydroxymethyl group. However, the introduction of the primary catalytic calcium ion leads to a stable chair conformer Ca−Cell−Ca species that is 7 kcal mol^{-1} lower in energy than the unbound cellulose state (Cell + 2Ca). In this conformation, the calcium ion frees up the hydroxymethyl group to rotate and form a highly stable chair conformer, where the OH strongly binds to the primary catalytic calcium ion near the glycosidic bond reaction center. Just as in the previous catalytic cycle, at low concentrations of the Ca-bound species the rates are measured with respect to the unbound state, thus resulting in an apparent rate constant of kK_1K_2 and an apparent activation energy of 41 kcal mol^{-1}. The observed rate order in this cycle would be second-order in Ca and first-order in Cell, which is in agreement with the experiments.

In configuration 2 (Figure 6B), the Ca−Cell−Ca boat conformer reactant is 15 kcal mol^{-1} uphill in energy versus 17 kcal mol^{-1} for the boat conformer intermediate in the single calcium case (not shown). As shown in Figure 5F, the secondary calcium ion breaks a strong intramolecular H-bond (circled green in Figure 5D), which promotes the conformational change from the chair structure to the boat structure and, in addition, the facile cleavage of the glycosidic bond. This is visible in the calculated activation barrier, which is ~3 kcal mol^{-1} lower than the calculated barrier for the single-calcium case (50 versus 53 kcal mol^{-1}, respectively). Such a difference is in good agreement with the observation that the promotional role of additional calcium involves simply breaking a H-bond. The calculated barrier for this cooperative cycle of 50 kcal mol^{-1} also agrees well with the experimentally measured

https://dx.doi.org/10.1021/jacsau.0c00092
JACS Au 2021, 1, 272−281

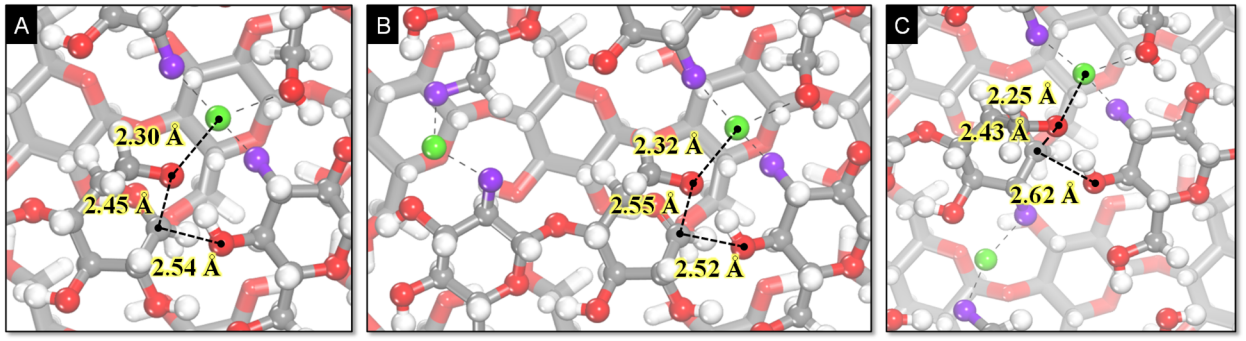

Figure 7. Optimized geometries for the transglycosidic bond cleavage transition states. (A) The single-calcium catalytic transition state. (B) The cooperative calcium-cycle transition state from configuration 1. (C) The cooperative calcium-cycle transition state from configuration 2.

barrier of 48.7 ± 2.8 kcal mol^{-1} for the calcium-catalyzed CD breakdown reported in the earlier section.

The structure of the optimized transition state in Figure 7A for the single calcium catalytic cycle has geometrical features (bond distances) near the reaction center that are similar to those observed for the optimized transition states in the cooperative calcium catalytic cycles shown in Figure 7B and C. This suggests that the additional Ca ion plays only a secondary role in lowering the activation barriers.

The above results and analysis suggest that a cooperative calcium mechanism should dominate based on its lower activation barrier. However, at very low concentrations of calcium it is likely that Ca−Cell species would have a higher concentration than that of Ca−Cell−Ca such that the cooperative mechanism may not dominate. At higher concentrations, the contribution of the cooperative cycle would likely increase. The observation of a noninteger rate order suggests that eq 22 in the Supporting Information may be a better kinetic model for cellulose activation. A rate order of ∼1.7 also suggests that at the chosen reaction conditions and calcium dopant levels the dual-calcium mechanism dominates over the single-calcium mechanism.

CONCLUSIONS

Millisecond reaction kinetics together with first-principle density functional theory calculations indicate that calcium-catalyzed cellulose activation can proceed via a mechanism involving single- and cooperative-calcium-catalyzed glycosidic bond activation. Temporally resolved conversion data of the cellulose surrogate, α-cyclodextrin, revealed a catalyzed acceleration of cellulose activation in the presence of calcium as well as an approximately second-order rate dependence of the calcium ion. Experiments also indicated a lower activation energy barrier for the calcium-catalyzed glycosidic bond activation of 48.7 ± 2.8 kcal mol^{-1}. Overall rate expressions that account for the noncatalyzed and calcium-catalyzed mechanisms were derived. The kinetics of the calcium-catalyzed activation were evaluated using explicit cellulose crystal models and density functional theory calculations. For the single-calcium and cooperative-calcium mechanisms, DFT results suggest that one calcium ion plays a primary catalytic role of stabilizing the charge center of the transition state. However, in the cooperative mechanism an additional calcium ion was shown to play the secondary promotional role of disrupting the native H-bonding networks to enhance the reactivity. Such a cooperative mechanism explains the observed rate orders and is also the dominant mechanism of activation at the selected calcium dopant levels. This cooperative catalytic mechanism serves to significantly lower the temperature at which lignocellulosic materials become chemically accessible, either in nature or through engineered renewable-energy systems.

METHODS

Cyclodextrin Sample Preparation

Thin films of α-cyclodextrin samples were prepared via evaporative deposition on passivated carbon-steel heating elements. Heating elements were cleaned and passivated using a butane torch before cooling to ambient conditions. To 1.0 wt % solution of α-cyclodextrin prepared in HPLC-grade water was added the corresponding amount of $Ca(NO_3)_2{\cdot}4H_2O$ (0.1−0.5 mmol $Ca(NO_3)_2$ g_{CD}^{-1}), and the solution was thoroughly mixed to dope α-cyclodextrin with calcium. A 5.0 μL aliquot of the solution was pipetted on the center of the cleaned heating element, corresponding to 50 μg of α-cyclodextrin. Samples were then placed under vacuum at 25 in. Hg and 40 °C until the water evaporated and the film was formed. This deposition and drying technique was performed twice sequentially to generate 100 μg samples that were uniform circular films <20 μm in thickness and 3.0 mm in diameter.

Reaction Experiments

The reaction of the α-cyclodextrin films was performed using the method of pulse-heated analysis of solid and surface reactions (PHASR) by which reactant samples were subjected to rapid thermal pulses for prescribed temperatures and time intervals. A detailed design and description of the reactor performance has previously been described.[33] Reactant samples were placed in a sealed reactor chamber between two stainless-steel custom machined-reactor housings (an upper heating housing and a lower cooling housing). The upper reactor housing contained two electrical leads that contacted the heating element to transfer a uniform electric current and heat the sample. A 1000 Hz optical pyrometer measured the temperature of the sample and was integrated with a 2000 Hz PID controller to precisely control the reaction temperature.

Chemical Product Analysis

Quantification of the remaining α-cyclodextrin reactant after a thermal PHASR pulse was conducted via solvent extraction and liquid chromatography with light-scattering detection. Heating elements containing partially reacted samples were removed from the PHASR reactor and cut into a small circle containing only the sample film. The smaller heating element was then placed in a 1.5 mL PTFE filter vial, after which 350 μL of HPLC grade water was pipetted into each vial. Vials were shaken for about 1 min to ensure the complete dissolution of α-cyclodextrin. The remaining heating element was then removed from the vial, and the filter plunger was depressed to remove any remaining particulate. Then, 100 μL of the filtered sample was injected into a high-performance liquid chromatograph (HPLC, Shimadzu Prominence) with a carbohydrate separation

https://dx.doi.org/10.1021/jacsau.0c00092
JACS Au 2021, 1, 272−281

column (Agilent Na Hi-Plex, PN: 1171−6140), a light-scattering detector (ELSD-LTII), and a water mobile phase. Quantification of the α-cyclodextrin peak from the ELSD for PHASR pulses of increasing lengths yielded the consumption of the reactant with time.

Computational Methods

All the calculations reported herein were carried out using periodic plane-wave density functional theory in the Vienna Ab Initio Simulation Program (VASP)[42−44] and the generalized gradient approximation (GGA) functional developed by Perdew, Burke, and Ernzerhof (PBE).[45] The D2 method developed by Grimme, which can account for two-body dispersive interactions, was applied in all calculations.[46,47] Plane waves with an energy cutoff of 396 eV were used based on projector augmented wave potentials (PAW).[48] A 1 × 1 × 1 *k*-point grid was found to be sufficient for the system based on energy convergence calculations.[49] The calculations were performed until self-consistent field calculations and the geometric optimization converged to 10^{-6} eV and a force of 0.05 eV $Å^{-1}$. To evaluate the barriers for a mechanism, the climbing NEB method was used to generate intermediate images for the pathway and subsequently optimize the pathway with a force tolerance of 0.2 eV $Å^{-1}$.[50,51] The transition state was then obtained using the dimer method, as developed by Henkelman, with a force tolerance of 0.05 eV $Å^{-1}$.[52] To evaluate diffusion, NVT AIMD simulations were performed with the same functionals and dispersion corrections. The time-step for the AIMD simulations was 1 fs. The temperature was maintained at 700 K using a Nosè−Hoover thermostat.[53,54]

Computational Model

A 1 × 2 × 2 supercell of the cellulose Iβ crystal was used to examine the most stable binding sites for calcium ions. The model was slightly modified to simulate the reactions such that it consisted of a cellulose sheet with a degree of polymerization of three that was sandwiched between two periodically extending cellulose sheets to reproduce the environment in a cellulose Iβ crystal. This modification of the reaction sheet was carried out because in a periodic model it is not possible cleave the cellulose chain unless it is clipped to have a finite degree of polymerization. The above-described model to simulate reactions was enclosed in a periodic cell with lattice parameters of a = 16.352 Å, b = 16.402 Å, and c = 20.760 Å. The value of ϒ = 96.55° was used to closely match the crystal parameter observed in experimental XRD studies.[55,56]

■ ASSOCIATED CONTENT

Supporting Information

The Supporting Information is available free of charge at https://pubs.acs.org/doi/10.1021/jacsau.0c00092.

Raw tabulated conversion data for calcium-incorporated samples of α-cyclodextrin, validation of the second-order dependence with calcium, confirmation of the effect of the nitrate counterion, derivation for the rate experssions of catalytic cycles, and additional structures of intermediate species and calcium binding sites(PDF)

■ AUTHOR INFORMATION

Corresponding Author

Paul J. Dauenhauer − *Department of Chemical Engineering and Materials Science, University of Minnesota, Minneapolis, Minnesota 55455, United States;* orcid.org/0000-0001-5810-1953; Email: hauer@umn.edu

Authors

Gregory G. Facas − *Department of Chemical Engineering and Materials Science, University of Minnesota, Minneapolis, Minnesota 55455, United States*

Vineet Maliekkal − *Department of Chemical Engineering and Materials Science, University of Minnesota, Minneapolis, Minnesota 55455, United States*

Cheng Zhu − *Department of Chemical Engineering and Materials Science, University of Minnesota, Minneapolis, Minnesota 55455, United States*

Matthew Neurock − *Department of Chemical Engineering and Materials Science, University of Minnesota, Minneapolis, Minnesota 55455, United States*

Complete contact information is available at: https://pubs.acs.org/10.1021/jacsau.0c00092

Author Contributions

‡Authors contributed equally

Notes

The authors declare no competing financial interest.

■ ACKNOWLEDGMENTS

We acknowledge support from the U.S. Department of Energy, Office of Basic Energy Science Catalysis (DE-SC0016346). We also acknowledge valuable insights from discussions with Dr. Manish Shetty and Professor Omar Abdelrahman.

■ REFERENCES

(1) Huber, G. W.; Iborra, S.; Corma, A. Synthesis of Transportation Fuels from Biomass: Chemistry, Catalysts, and Engineering. *Chem. Rev.* **2006**, *106*, 4044−4098.

(2) Demirbas, A.; Arin, G. An Overview of Biomass Pyrolysis. *Energy Sources* **2002**, *24*, 471−482.

(3) Bridgwater, A. V. Renewable fuels and chemicals by thermal processing of biomass. *Chem. Eng. J.* **2003**, *91*, 87−102.

(4) Chundawat, S. P. S.; Beckham, G. T.; Himmel, M. E.; Dale, B. E. Deconstruction of Lignocellulosic Biomass to Fuels and Chemicals. *Annu. Rev. Chem. Biomol. Eng.* **2011**, *2*, 121−145.

(5) Lédé, J. Cellulose pyrolysis kinetics: An historical review on the existence and role of intermediate active cellulose. *J. Anal. Appl. Pyrolysis* **2012**, *94*, 17−32.

(6) Alonso, D. M.; Bond, J. Q.; Dumesic, J. A. Catalytic conversion of biomass to biofuels. *Green Chem.* **2010**, *12*, 1493−1513.

(7) De, S.; Saha, B.; Luque, R. Hydrodeoxygenation processes: Advances on catalytic transformations of biomass-derived platform chemicals into hydrocarbon fuels. *Bioresour. Technol.* **2015**, *178*, 108−118.

(8) Vinu, R.; Broadbelt, L. J. A mechanistic model of fast pyrolysis of glucose-based carbohydrates to predict bio-oil composition. *Energy Environ. Sci.* **2012**, *5*, 9808−9826.

(9) Mayes, H. B.; Broadbelt, L. J. Unraveling the Reactions that Unravel Cellulose. *J. Phys. Chem. A* **2012**, *116*, 7098−7106.

(10) Mettler, M. S.; Vlachos, D. G.; Dauenhauer, P. J. Top ten fundamental challenges of biomass pyrolysis for biofuels. *Energy Environ. Sci.* **2012**, *5*, 7797−7809.

(11) Maduskar, S.; Facas, G. G.; Papageorgiou, C.; Williams, C. L.; Dauenhauer, P. J. Five Rules for Measuring Biomass Pyrolysis Rates: Pulse-Heated Analysis of Solid Reaction Kinetics of Lignocellulosic Biomass. *ACS Sustainable Chem. Eng.* **2018**, *6*, 1387−1399.

(12) SriBala, G.; Carstensen, H.-H.; Van Geem, K. M.; Marin, G. B. Measuring biomass fast pyrolysis kinetics: State of the art. *WIREs Energy Environ.* **2019**, *8*, e326.

(13) Hosoya, T.; Nakao, Y.; Sato, H.; Kawamoto, H.; Sakaki, S. Thermal degradation of methyl β-D-glucoside. A theoretical study of plausible reaction mechanisms. *J. Org. Chem.* **2009**, *74*, 6891−6894.

(14) Seshadri, V.; Westmoreland, P. R. Concerted reactions and mechanism of glucose pyrolysis and implications for cellulose kinetics. *J. Phys. Chem. A* **2012**, *116*, 11997−12013.

(15) Hosoya, T.; Sakaki, S. Levoglucosan formation from crystalline cellulose: Importance of a hydrogen bonding network in the reaction. *ChemSusChem* **2013**, *6*, 2356−2368.
(16) Seshadri, V.; Westmoreland, P. R. Roles of hydroxyls in the noncatalytic and catalyzed formation of levoglucosan from glucose. *Catal. Today* **2016**, *269*, 110−121.
(17) Agarwal, V.; Dauenhauer, P. J.; Huber, G. W.; Auerbach, S. M. Ab initio dynamics of cellulose pyrolysis: Nascent decomposition pathways at 327 and 600 C. *J. Am. Chem. Soc.* **2012**, *134*, 14958−14972.
(18) Zhu, C.; Krumm, C.; Facas, G. G.; Neurock, M.; Dauenhauer, P. J. Energetics of cellulose and cyclodextrin glycosidic bond cleavage. *React. Chem. Eng.* **2017**, *2*, 201−214.
(19) Maliekkal, V.; Maduskar, S.; Saxon, D. J.; Nasiri, M.; Reineke, T. M.; Neurock, M.; Dauenhauer, P. J. Activation of Cellulose via Cooperative Hydroxyl-Catalyzed Transglycosylation of Glycosidic Bonds. *ACS Catal.* **2019**, *9*, 1943−1955.
(20) Westmoreland, P. R. Pyrolysis kinetics for lignocellulosic biomass-to-oil from molecular modeling. *Curr. Opin. Chem. Eng.* **2019**, *23*, 123−129.
(21) Mellmer, M. A.; Sanpitakseree, C.; Demir, B.; Bai, P.; Ma, K.; Neurock, M.; Dumesic, J. A. Solvent-Enabled Control of Reactivity for Liquid-Phase Reactions of Biomass-Derived Compounds. *Nat. Catal.* **2018**, *1*, 199−207.
(22) Mellmer, M. A.; Sanpitakseree, C.; Demir, B.; Ma, K.; Elliott, W. A.; Bai, P.; Johnson, R. L.; Walker, T. W.; Shanks, B. H.; Rioux, R. M.; et al. Effects of Chloride Ions in Acid-Catalyzed Biomass Dehydration Reactions in Polar Aprotic Solvents. *Nat. Commun.* **2019**, *10*, 1132.
(23) Agblevor, F. A.; Besler, S. Inorganic compounds in biomass feedstocks. 1. Effect on the quality of fast pyrolysis oils. *Energy Fuels* **1996**, *10*, 293−298.
(24) Sekiguchi, Y.; Shafizadeh, F. The Effect of Inorganic Additives on the Formation, Composition, and Combustion of Cellulosic Char. *J. Appl. Polym. Sci.* **1984**, *29*, 1267−1286.
(25) Muller-Hagedorn, M.; Bockhorn, H.; Krebs, L.; Muller, U. A comparative kinetic study on the pyrolysis of three different wood species. *J. Anal. Appl. Pyrolysis* **2003**, *68−69*, 231−249.
(26) Carvalho, W. S.; Cunha, I. F.; Pereira, M. S.; Ataíde, C. H. Thermal decomposition profile and product selectivity of analytical pyrolysis of sweet sorghum bagasse: Effect of addition of inorganic salts. *Ind. Crops Prod.* **2015**, *74*, 372−380.
(27) Zhu, C.; Maduskar, S.; Paulsen, A. D.; Dauenhauer, P. J. Alkaline-Earth-Metal-Catalyzed Thin-Film Pyrolysis of Cellulose. *ChemCatChem* **2016**, *8*, 818−829.
(28) Patwardhan, P. R.; Satrio, J. A.; Brown, R. C.; Shanks, B. H. Influence of inorganic salts on the primary pyrolysis products of cellulose. *Bioresour. Technol.* **2010**, *101*, 4646−4655.
(29) Quiroz, N. R.; Norton, A. M.; Nguyen, H.; Vasileiadou, E. S.; Vlachos, D. G. Homogeneous Metal Salt Solutions for Biomass Upgrading and Other Select Organic Reactions. *ACS Catal.* **2019**, *9*, 9923−9952.
(30) Arora, J. S.; Chew, J. W.; Mushrif, S. H. Influence of Alkali and Alkaline-Earth Metals on the Cleavage of Glycosidic Bonds in Biomass Pyrolysis: A DFT study using Cellobiose as a Model Compound. *J. Phys. Chem. A* **2018**, *122*, 7646−7658.
(31) Mayes, H. B.; Tian, J.; Nolte, M. W.; Shanks, B. H.; Beckham, G. T.; Gnanakaran, S.; Broadbelt, L. J. Sodium Ion Interactions with Aqueous Glucose: Insights from Quantum Mechanics, Molecular Dynamics, and Experiment. *J. Phys. Chem. B* **2014**, *118* (8), 1990−2000.
(32) Saddawi, A.; Jones, J. M.; Williams, A. Influence of alkali metals on the kinetics of the thermal decomposition of biomass. *Fuel Process. Technol.* **2012**, *104*, 189−197.
(33) Krumm, C.; Pfaendtner, J.; Dauenhauer, P. J. Millisecond Pulsed Films Unify the Mechanisms of Cellulose Fragmentation. *Chem. Mater.* **2016**, *28*, 3108−3114.
(34) Paulsen, A. D.; Mettler, M. S.; Dauenhauer, P. J. The role of sample dimension and temperature in cellulose pyrolysis. *Energy Fuels* **2013**, *27*, 2126−2134.
(35) Mettler, M. S.; Mushrif, S. H.; Paulsen, A. D.; Javadekar, A. D.; Vlachos, D. G.; Dauenhauer, P. J. Revealing pyrolysis chemistry for biofuels production: Conversion of cellulose to furans and small oxygenates. *Energy Environ. Sci.* **2012**, *5*, 5414−5424.
(36) Maliekkal, V.; Dauenhauer, P. J.; Neurock, M. Glycosidic CO Bond Activation in Cellulose Pyrolysis: Alpha Versus Beta and Condensed Phase Hydroxyl-Catalytic Scission. *ACS Catal.* **2020**, *10*, 8454−8464.
(37) Jensen, P. A.; Frandsen, F. J.; Dam-Johansen, K.; Sander, B. Experimental Investigation of the Transformation and Release to Gas Phase of Potassium and Chlorine during Straw Pyrolysis. *Energy Fuels* **2000**, *14*, 1280−1285.
(38) Burés, J. A simple graphical method to determine the order in catalyst. *Angew. Chem., Int. Ed.* **2016**, *55*, 2028−2031.
(39) Nielsen, L. P. C.; Stevenson, C. P.; Blackmond, D. G.; Jacobsen, E. N. Mechanistic investigation leads to a synthetic improvement in the hydrolytic kinetic resolution of terminal epoxides. *J. Am. Chem. Soc.* **2004**, *126*, 1360−1362.
(40) Bugg, C. E. Calcium binding to carbohydrates. Crystal structure of a hydrated calcium bromide complex of lactose. *J. Am. Chem. Soc.* **1973**, *95*, 908−913.
(41) Cook, W. J.; Bugg, C. E. Calcium Binding to Galactose. Crystal Structure of a Hydrated a-Galactose-Calcium Bromide Complex. *J. Am. Chem. Soc.* **1973**, *95*, 6442−6446.
(42) Kresse, G.; Furthmüller, J. Efficient iterative schemes for *ab initio* total-energy calculations using a plane-wave basis set. *Phys. Rev. B: Condens. Matter Mater. Phys.* **1996**, *54*, 11169−11186.
(43) Kresse, G.; Hafner, J. Ab initio molecular dynamics for liquid metals. *Phys. Rev. B: Condens. Matter Mater. Phys.* **1993**, *47*, 558−561.
(44) Kresse, G.; Hafner, J. Ab initio molecular-dynamics simulation of the liquid-metal−amorphous-semiconductor transition in germanium. *Phys. Rev. B: Condens. Matter Mater. Phys.* **1994**, *49*, 14251−14269.
(45) Perdew, J. P.; Burke, K.; Ernzerhof, M. Generalized gradient approximation made simple. *Phys. Rev. Lett.* **1996**, *77*, 3865−3868.
(46) Grimme, S. Semiempirical GGA-Type Density Functional Constructed with a Long-Range Dispersion Correction. *J. Comput. Chem.* **2006**, *27*, 1787−1799.
(47) Grimme, S. Density functional theory with London dispersion corrections. *Wiley Interdiscip. Rev.: Comput. Mol. Sci.* **2011**, *1*, 211−228.
(48) Kresse, G.; Joubert, D. From ultrasoft pseudopotentials to the projector augmented-wave method. *Phys. Rev. B: Condens. Matter Mater. Phys.* **1999**, *59*, 1758−1775.
(49) Pack, J. D.; Monkhorst, H. J. 'special points for Brillouin-zone integrations'-a reply. *Phys. Rev. B* **1977**, *16*, 1748−1749.
(50) Henkelman, G.; Uberuaga, B. P.; Jónsson, H. A climbing image nudged elastic band method for finding saddle points and minimum energy paths. *J. Chem. Phys.* **2000**, *113*, 9901−9904.
(51) Henkelman, G.; Jónsson, H. Improved tangent estimate in the nudged elastic band method for finding minimum energy paths and saddle points. *J. Chem. Phys.* **2000**, *113*, 9978−9985.
(52) Henkelman, G.; Jónsson, H. A dimer method for finding saddle points on high dimensional potential surfaces using only first derivatives. *J. Chem. Phys.* **1999**, *111*, 7010−7022.
(53) Nosè, S. A unified formulation of the constant temperature molecular dynamics method. *J. Chem. Phys.* **1984**, *81*, 511−519.
(54) Hoover, W. G. Canonical dynamics: Equilibrium phase-space distributions. *Phys. Rev. A: At., Mol., Opt. Phys.* **1985**, *31*, 1695−1697.
(55) Langan, P.; Sukumar, N.; Nishiyama, Y.; Chanzy, H. Synchrotron X-ray structures of cellulose Iβ and regenerated cellulose II at ambient temperature and 100 K. *Cellulose* **2005**, *12*, 551−562.
(56) Nishiyama, Y.; Langan, P.; Chanzy, H. Crystal structure and hydrogen-bonding system in cellulose Iβ from synchrotron X-ray and neutron fiber diffraction. *J. Am. Chem. Soc.* **2002**, *124*, 9074−9082.

https://dx.doi.org/10.1021/jacsau.0c00092
JACS Au 2021, 1, 272−281